Nanoscale

PAPER

View Article Online
View Journal | View Issue

Cite this: *Nanoscale*, 2025, **17**, 28091

Multifunctional and stimuli-responsive ionic liquid-polymeric hydrogel: a promising platform for co-drug delivery in cancer treatment

Ishani Pandya,[a] Vidhi Joshi,[a] Sugam Kumar,[b] Vinod K. Aswal,[b] Naina Raje,[c] Muzammil Kuddushi,[d,e] Xuehua Zhang *[e] and Naved Malek *[a]

Designing intelligent drug delivery systems that offer high drug loading, site-specific release, and improved therapeutic outcomes is crucial to overcome the limitations of conventional cancer treatments. This study presents a novel pH-responsive hydrogel developed by integrating a biocompatible ionic liquid (IL), [TMG][Ol], into a polymeric matrix to enable the co-delivery of the chemotherapeutic drug 5-fluorouracil (5-FU) and heparin (Hp), aimed at cancer treatment and metastasis inhibition. Structural and surface characterization studies were performed using XPS, FTIR, SANS and FE-SEM, confirming the successful formation of the composite network, while thermal stability was evaluated through DSC analysis. Rheological analysis demonstrated robust mechanical strength, while thixotropic studies validated its injectability, supporting minimally invasive delivery. The hydrogel also exhibited notable self-healing and adhesive properties. [TMG][Ol] incorporation enhanced drug loading capacity by ~2.5-fold over the IL-free hydrogel. Drug release studies confirmed pH-responsive behaviour, with over 90.2% of 5-FU and 77.6% of Hp released at pH 5.2 within 48 hours, while release remained below 60% at physiological pH, minimizing off-target effects. Biocompatibility was validated using HaCaT cells, showing over 95% cell viability after 48 hours of exposure. *In vitro* cytotoxicity assays revealed a dose-dependent reduction in cancer cell viability, with significant inhibition observed in MCF-7 and HeLa cells, revealing significant therapeutic efficacy. Furthermore, anti-metastatic activity assessed *via* a scratch assay in HeLa cells showed a substantial reduction in cell migration compared to the control. These findings underscore the potential of the developed IL-based hydrogel as a promising dual-delivery platform with targeted, sustained release, strong therapeutic potential, and minimal toxicity to healthy cells, offering a new avenue for effective cancer therapy and metastasis suppression.

Received 6th August 2025,
Accepted 27th October 2025

DOI: 10.1039/d5nr03333k

rsc.li/nanoscale

1. Introduction

Cancer remains one of the most devastating diseases worldwide, accounting for approximately 9.6 million deaths in 2018 alone.[1] Current treatment options include surgery, chemotherapy, radiotherapy, and immunotherapy. Although chemotherapy can be effective, its broader application is often limited by adverse drug reactions, a low therapeutic index, drug resistance, and poor targeting efficiency.[2] In recent years, advanced drug delivery strategies have been explored to improve the efficacy of chemotherapy while minimizing its side effects. Among these, nanotechnology has shown great promise by enabling the selective accumulation of drugs in tumor tissues through both passive and active targeting mechanisms.[3] A wide variety of drug delivery vehicles have been developed to enhance bioavailability, improve drug stability, and achieve site-specific drug release. These include nanoparticles, vesicles,[4] metal–organic frameworks (MOFs),[5] liposomes,[6] and hydrogels.[7] Among them, hydrogels have garnered significant attention in cancer therapy due to their high water content, tunable cross-linked polymer networks, excellent biocompatibility, negligible cytotoxicity, and superior drug-encapsulation capabilities.[7,8] These properties make

[a]*Ionic Liquids Research Laboratory, Department of Chemistry, Sardar Vallabhbhai National Institute of Technology, Surat-395007, Gujarat, India. E-mail: navedmalek@chem.svnit.ac.in*
[b]*Solid State Physics Division, Bhabha Atomic Research Centre, Trombay, Mumbai 400085, India*
[c]*Analytical Chemistry Division, Bhabha Atomic Research Centre, Trombay, Mumbai 400085, India*
[d]*School of Civil Environmental Engineering and Geography Science, Ningbo University, Ningbo 315211, China*
[e]*Department of Chemical and Materials Engineering, University of Alberta, Alberta T6G 1H9, Canada. E-mail: xuehua.zhang@ualberta.ca*

hydrogels highly suitable for controlled and localized drug delivery, contributing to their widespread use in recent cancer treatment research.[5,6]

Hydrogels can load both hydrophilic and hydrophobic drugs and respond to external stimuli like pH, temperature, and ionic strength, enabling controlled and sustained drug release. Hydrogels can be formulated using natural polymers such as chitosan and sodium alginate (SA), synthetic polymers like poly(vinyl alcohol) (PVA), or a blend of both to combine their respective advantages. Synthetic polymers have high processability and mechanical characteristics, while natural polymers are biodegradable, biocompatible, and also low in toxicity. Blends of natural and synthetic polymers, known as biosynthetic or bioartificial polymers, have gained popularity in biomedical applications due to their superior thermal, mechanical, and biocompatible properties relative to single-component materials.[1]

Among synthetic hydrogel-forming polymers, PVA stands out for its excellent biocompatibility, chemical resistance, biodegradability, and large-scale producibility, making its hydrogels widely used in synthetic cartilage, surgical devices, and drug delivery systems.[2,3] Whereas SA is a biocompatible, biodegradable, and cost-effective natural polymer derived from seaweed and is composed of β-D-mannuronic acid and α-L-guluronic acid units and is commonly used in biomedical gels for its good gel-forming ability.[4] The SA–PVA hydrogel combines the advantages of both polymers, and many researchers have focused on its preparation and application in drug delivery.[5,6] However, the application of the SA–PVA hydrogel is limited by its poor gel strength, non-injectability and low drug loading capacity,[7] which can be enhanced through various strategies such as incorporating nanoclays,[8] nanoparticles[9] or ionic liquids.[10]

Recently, multifunctional and stimuli-responsive polymeric hydrogels have attracted significant attention as advanced drug delivery systems due to their capability to respond to environmental changes and provide controlled release of therapeutic agents. Rashidzadeh *et al.* developed pH-sensitive hydrogels to provide site-specific and sustained release of therapeutic agents, making them highly suitable for cancer and malaria treatment.[11] A dual pH- and magnetic-responsive hydrogel has been reported for the co-delivery of chloroquine and methotrexate, exhibiting controlled and stimuli-induced drug release behaviour.[12] Chen *et al.* developed a doxorubicin-delivering hydrogel from Pluronic F127, enhancing its thermo-responsive properties with hyaluronic acid and boosting its mechanical characteristics using hexamethylene diisocyanate.[13] Physically cross-linking poly(methacrylic acid) with hexadecyltrimethylammonium chloride micelles yields a hydrogel that exhibits shape memory, load-bearing and self-healing capabilities, along with responsiveness to salt, heat, and pH changes.[14]

Surfactants are valuable additives due to their tunable, biocompatible nature and their ability to self-assemble and transport drug molecules of varying polarity. A modern class of surfactants with ionic liquid characteristics, known as surface-active ionic liquids (SAILs), represents a promising category of additives with precisely tunable properties, making them ideal for engineering stimuli-responsive hydrogels.[15,16] For example, SAILs based on [TMG][Ol] exhibit excellent biocompatibility, amphiphilic behaviour, and compatibility with hydrophilic polymers.[17] These compounds can be synthesized *via* a simple acid–base neutralization reaction, without the use of harmful solvents, aligning with the principles of green chemistry.[17] While potential degradation products must be considered, the $[TMG]^+$ cation derived from guanidine exhibits low cytotoxicity at moderate concentrations,[18] and oleate, a naturally occurring fatty acid, is well known for its biomedical safety and beneficial roles.[7] The non-aromatic and strongly basic nature of $[TMG]^+$ facilitates hydrogen bonding with polymer chains, enabling hydrogel formation without the need for toxic cross-linkers.[17] Owing to its SAIL characteristics, [TMG][Ol] also plays a crucial role in modulating the hydrogel microstructure, porosity, diffusion behaviour, and drug release kinetics, factors essential for precision-targeted drug delivery.[4]

In this study, we developed a multifunctional, pH-responsive hydrogel by incorporating the biocompatible ionic liquid [TMG][Ol] into a PVA–SA polymeric matrix for the co-delivery of 5-fluorouracil (5-FU) and heparin (Hp). The unique physicochemical properties of [TMG][Ol], including its amphiphilicity, biocompatibility, and hydrogen-bonding capability, facilitate stable hydrogel formation without toxic crosslinkers while also enhancing drug loading and controlled release. The resulting hydrogel demonstrates robust mechanical strength, along with self-healing and adhesive properties, and selective drug release in acidic tumor microenvironments. This platform holds strong potential for localized, sustained cancer therapy with reduced systemic toxicity and improved anti-metastatic outcomes.

2. Experimental work

2.1. Materials

Sodium alginate (SA), poly(vinyl alcohol) (PVA) (M_w = 9000–10 000, 80% hydrolysed) and 1,1,3,3-tetramethylguanidine (TMG) were purchased from Sigma-Aldrich, USA. 5-Fluorouracil (5-FU) (>99.0%) was obtained from Tokyo Chemical Industry (TCI), Japan. Oleic acid and heparin sodium salt (Hp) (150 IU mg^{-1}) were bought from SRL (Sisco Research Laboratory, India). All of the chemicals were used as supplied and were of reagent grade. Double-distilled deionized water was used for every stage of the experiment.

2.2. Synthesis of [TMG][Ol]

[TMG][Ol] was synthesized using an established method.[19] TMG and oleic acid were combined in a molar ratio of 1 : 1 to produce the IL. An equal molar amount of TMG was drip-fed into a dry flask containing oleic acid while being agitated on a magnetic stirrer using a constant pressure funnel. The flask was placed in an ice bath. To remove any unreacted TMG and oleic acid, the mixture was vacuum-dried at 70 °C after two hours. Finally, at room temperature, a highly viscous, pale-

yellow liquid formed. Prior to measurement, the IL was vacuum-stored and dried at reduced pressure. The structure of [TMG][Ol] was characterized by nuclear magnetic resonance hydrogen spectroscopy (^{1}H NMR, Bruker AVANCE NEO 500 MHz, ^{13}C NMR, JEOL 400 Hz, Delta 6.0) and Fourier transform infrared spectroscopy (FT-IR, Jasco6000).

^{1}H NMR (ppm): δ 0.88 (t, 3H, CH_3), 1.25 (m, 20H, CH_2), 1.57 (m, 2H, $C\underline{H}_2CH_2COO^-$), 2.02 (m, 4H, $C\underline{H}_2CH{=}CHC\underline{H}_2$), 2.18 (t, 2H, $C\underline{H}_2COO^-$), 2.97 (s, 12H, NCH_3), 5.33 (m, 2H, CH=CH), 6.4 (s, 2H, $C{=}NH_2^+$).

^{13}C NMR (ppm): 14.24 (CH_3), 16.36–31.59 (CH_2), 41.06 (CH_3 of [TMG]), 133.32 (CH=CH), 158.93 ($C{=}NH_2^+$), 185.46 (C=O).

2.3. Preparation of the hydrogel

To prepare the hydrogel with varying IL ratios, an aqueous solution of [TMG][Ole] (at concentrations 100 times higher than the CMC) was used, to which fixed concentrations of PVA (2% w/v) and SA (2% w/v) were added. The mixture was then heated to 60 °C to achieve a homogeneous solution. After cooling at room temperature (25 °C), the solution formed a hydrogel (Fig. S1). As depicted in Table 1, the hydrogel formed effectively at an SA-PVA concentration of 2% w/v, whereas a lower concentration of SA–PVA resulted in a viscous solution.

2.4. Characterisation of the hydrogel

2.4.1. Fourier transform infrared spectroscopy (FTIR). A Jasco FTIR 6600 was used to study the interaction of [TMG][Ol], SA and PVA in forming the hydrogel. The spectra ranged from 400 to 4000 cm^{-1} and were scanned 45 times. The hydrogel samples were lyophilized prior to FTIR analysis to remove the residual moisture.

2.4.2. X-ray photoelectron spectroscopy (XPS). A Thermo Scientific NEXA surface analyser was used to assess chemical composition within the range of 0 to 1350 eV by XPS. XPS analysis confirmed the successful synthesis of the IL-SA–PVA hydrogel and the effective loading of the drug within the hydrogel matrix.

2.4.3. Small-angle neutron scattering (SANS). Using a SANS-I diffractometer, SANS studies were conducted at the Guide Tube Laboratory, Dhruva Reactor, Bhabha Atomic Research Centre in Mumbai, India. We examined the experimental scattering data using a range of fitting models working with the SasView analytical program.

2.4.4. Differential scanning calorimetry (DSC). The thermal behaviour of the [TMG][Ol], IL-SA–PVA gel and 5-FU/Hp@IL-SA–PVA gel was analysed using a DSC 3 STARe system from Mettler Toledo. The DSC study was carried out in the temperature range from 25 °C to 150 °C at a continuous heating rate of 10 °C min^{-1}.

2.4.5. Morphology analysis of the hydrogels. The SEM images of hydrogels and drug-loaded hydrogels were captured using a QUANTA 200 FESEM. After drying at ambient temperature, the samples were attached to a copper disk with double-sided carbon tape. The samples were then coated with gold.

2.5. Swelling equilibrium study

The swelling behaviour of the IL-SA–PVA gel was evaluated in phosphate-buffered saline (PBS) solutions at pH 7.4 and pH 5.2. Pre-weighed dried hydrogel samples were enclosed in a dialysis membrane and immersed in each buffer solution to prevent material loss during swelling. The samples were withdrawn at predetermined time intervals, gently blotted to remove surface water, and weighed immediately. Eqn (1) was used to obtain the equilibrium-swelling ratio of the hydrogel.

$$\text{Swelling ratio} = \frac{W_s}{W_d} \quad (1)$$

where W_s and W_d are the swollen and dry weights, respectively. Equilibrium swelling was considered when no significant change in the swelling ratio was observed between consecutive time points.

2.6. Mechanical properties of the hydrogel through rheology

The mechanical properties of the present hydrogel were measured *via* a rheological study. An Anton Paar MCR 92 rheometer was used for this investigation, and parallel plates with 25 mm diameter and 0.5 mm spacing were used. Using a fixed 1 rad s^{-1} angular frequency, the modulus was evaluated in the strain sweep test between 0.1 and 10% strain. The hydrogel was then subjected to a frequency sweep test with an increasing angular frequency from 0.1 to 100 rad s^{-1} against modulus while maintaining a constant strain of 1%. The hydrogel viscosity was measured at shear rates ranging from 0.1 to 100 1 s^{-1}.

2.7. Stability evaluation under the influence of pH

The *in vitro* degradation behaviour of the [TMG][Ol], SA–PVA gel and IL-SA–PVA gel was evaluated using PBS solutions under acidic and physiological pH conditions. The study involved visual inspection of the samples over time. Further analysis of the samples was conducted using FTIR to investigate changes in the chemical structure. The degradation profile of the IL-SA–PVA gel was quantitatively examined by measuring the remaining weight percentage at pH 5.2 and 7.4. Pre-weighed dried hydrogels were enclosed in a dialysis membrane and immersed in 10 mL of PBS of pH 5.2 and 7.4. The samples were taken out at predetermined intervals, surface-dried, and weighed. Eqn (2) was used for calculating the remaining weight (%).

$$\text{Remaining weight}\,(\%) = \frac{W_t}{W_0} \times 100 \quad (2)$$

where W_t and W_0 are the weights of the hydrogel at time t and the initial weight, respectively. The tests were conducted in triplicate.

Table 1 Composition used to prepare 1 mL hydrogel

Composition	[TMG][Ol]	SA	PVA	Results
SA–PVA	—	2% w/v	2% w/v	Viscous solution
SA–PVA	—	3% w/v	3% w/v	gel
IL-SA	60 mM	2% w/v	—	Loose gel
IL-SA–PVA	60 mM	2% w/v	1% w/v	Loose gel
IL-SA–PVA	60 mM	2% w/v	2% w/v	gel

2.8. *In vitro* biocompatibility and cytotoxicity assessment

The HaCaT cell line was utilized to assess the biocompatibility of the hydrogel using the commonly used MTT assay. HaCaT cells, derived from adult human skin, are a reliable keratinocyte cell line. After allowing the cells to grow overnight in 96-well plates, various quantities of hydrogel samples were introduced. Untreated cells served as the control. After incubation for 24 hours, MTT solution (0.5 mg mL^{-1}) was added to the cell cultures and further incubated for 2 h. After a 10-minute incubation time at 37 °C, microplate readers were used to measure absorbance at 540 nm in the cell well plates. Cell viability was determined by comparing the results with those of negative and positive control materials. The same procedure was used to evaluate the cytotoxicity of 5-FU/Hp-loaded hydrogels in breast cancer (MCF-7) and cervical cancer (HeLa) cell lines, aiming to assess drug efficacy and determine IC_{50} values.

2.9. Drug loading efficiency within the hydrogel

To load 5-FU and Hp (hydrophilic drugs) into the hydrogel, we used an effective dialysis membrane approach. Before usage, 17.5 mm dialysis membranes with a molecular weight cut-off (MWCO) of 12–14 kDa were immersed in distilled water for 24 hours. The hydrogel was cautiously placed onto the dialysis membrane after being precisely measured. The assembly was placed in a drug solution at a specified concentration for 24 hours at room temperature. The evaluation of the drug loading capacity in the hydrogel was carried out using drug absorption assays. Following a standard calibration curve, we ascertained the concentration of loaded drugs (5-FU and Hp) in the gel.

2.10. *In vitro* release studies

The dialysis membrane containing the drug-loaded hydrogel was submerged in 20 mL of a pH 5.2 buffer solution at 37 °C. The same method was performed using a 7.4 pH buffer solution. To quantify the released drug, 500 μL of the release medium was taken out at periodic times. Additionally, an equivalent amount of PBS was added in order to maintain the previous volume. Following that, the samples were examined using UV-vis spectroscopy to ascertain the amount of drug released at various intervals. Experiments were carried out in triplicate.

2.11. *In vitro* scratch assay

Cell migration was evaluated *in vitro* using a scratch wound closure assay in cultured cells. HeLa cells were cultured in 96-well plates at 37 °C under a humidified atmosphere containing 5% CO_2 for 24 hours, using DMEM supplemented with 1% antibiotic solution and 10% fetal bovine serum (FBS). Untreated cells were referred to as control cells. After making a scratch with a 200 μl tip, the cells were treated with the formulation at the specified doses the next day. Images were taken at different periods within a 48-hour period. The gap was examined using ImageJ software. Three runs of each experiment were conducted.

3. Results and discussion

3.1. Characterization of [TMG][Ol] and the hydrogel

The successful synthesis of [TMG][Ol] was confirmed by comparing the ^{1}H NMR spectra of the starting materials, TMG and Ol, with that of the synthesized product. This analysis provides valuable insights into the chemical structure and purity of the synthesized IL (Fig. S2). In the ^{1}H NMR spectrum of TMG, two singlet peaks were observed at δ 2.7 and 5.1 ppm, corresponding to the methyl (–N–CH_3) and imino (C=NH) protons, respectively.[20] The spectrum of oleic acid exhibited a broad signal at δ ~11.0 ppm due to the carboxylic proton, along with typical aliphatic proton peaks between δ 0.8 and 2.5 ppm and olefinic protons appearing at δ 5.3–5.4 ppm.[21] Upon formation of [TMG][Ol], considerable spectral changes were observed. The disappearance of the –COOH proton signal of oleic acid indicated the acid–base neutralization reaction between TMG and oleic acid, which resulted in the formation of the carboxylate anion (oleate). In addition, a slight downfield shift of the protons of TMG suggested the protonation of the nitrogen atom in the guanidine moiety.

The cationic part of the IL consists of a central guanidinium moiety substituted with four methyl groups. The singlet at δ 2.97 ppm is assigned to the corresponding methyl protons (–NCH_3), integrating for 12 protons, confirming the presence of four methyl groups symmetrically attached to the nitrogen atoms. A broad singlet in the δ 6.4 ppm area indicates the two exchangeable protons of the protonated NH_2^+ group. The anionic component exhibits a set of signals typical of a long-chain unsaturated fatty acid: δ 0.88 (t, 3H) is attributed to the terminal methyl group (–CH_3), 1.25 (m, 20H) to the methylene protons (–CH_2–) along the saturated alkyl chain, 1.57 (m, 2H) to the C$H_2$$CH_2COO^-$ group, 2.02 (m, 4H) to the allylic methylene groups (–CH_2–) adjacent to the double bond, 2.18 (t, 2H) to CH_2COO^- and 5.33 (m, 2H) to the vinylic protons (–CH=CH–) of the *cis*-double bond, confirming the presence of unsaturation in the fatty acid chain. The integration values and multiplicity of the observed signals are in good agreement with the expected structure of [TMG][Ol], confirming the successful formation of the ionic liquid.

The ^{13}C NMR spectrum further verified the synthesis of [TMG][Ol] (Fig. S3), showing distinct carbon resonances at δ 14.24, 16.36, 17.42, 18.87, 21.12, 23.61, 24.16, 25.96, 27.29, and 31.59 ppm corresponding to the aliphatic carbons of the oleate chain, a signal at δ 133.32 ppm for the C=C carbon, and a peak at δ 185.46 ppm corresponding to the carboxylate carbon. The characteristic carbon of the C=N group from the guanidinium moiety appeared at δ 158.93 ppm. These results collectively confirm the successful formation of [TMG][Ol].

As illustrated in Table 1, increasing the concentration of both polymers leads to a rise in the viscosity of the system, ultimately transforming it into a hydrogel. This transformation

is attributed to the enhanced non-covalent interactions among [TMG][Ol], SA and PVA (Fig. 1B), which were confirmed by FTIR analysis.

Fig. 1A shows the FTIR spectra of the IL-SA–PVA gel, SA–PVA gel, SA, PVA and [TMG][Ol]. The spectra of [TMG][Ol] show a wide band at 3360–3292 cm^{-1}, indicating the presence of the C═NH_2^+ cationic group and olefinic C–H stretching in ILs occurs at 3005 cm^{-1}. A C–H stretching of methyl and methylene units is suggested by sharp peaks at 2921–2852 cm^{-1}. The carboxylate anion is confirmed by two bands – symmetric stretching at 1442–1411 cm^{-1} and asymmetric stretching at 1600–1554 cm^{-1}. Around 1658 cm^{-1}, the C═C stretching and C═N are seen; based on this spectrum, the successful synthesis of [TMG][Ol] is validated.[22] In the IL-SA–PVA gel spectrum, the –NH_2 group of [TMG][Ol] and the –OH groups of PVA and sodium alginate exhibit substantial hydrogen bonding, as evidenced by a broad band observed in the 3200–3400 cm^{-1} region that corresponds to overlapping O–H and N–H stretching vibrations. There were changes in the symmetric and asymmetric stretching vibrations of $–COO^-$ about 1610 cm^{-1} and 1420 cm^{-1}, respectively, which suggested electrostatic interactions. These results highlight the synergistic role of [TMG][Ol], PVA and SA in forming a crosslinked hydrogel with strong electrostatic and hydrogen bonding interactions.

The successful incorporation and stability of 5-FU and Hp within the 5-FU/Hp@IL-SA–PVA gel were primarily confirmed through FTIR spectroscopy, as indicated by the presence of characteristic peaks corresponding to the functional groups of 5-FU and Hp in the drug-loaded hydrogel. Fig. S4 shows the comparative FTIR spectra of the IL-SA–PVA gel, pure 5-FU, pure Hp and 5-FU/Hp@IL-SA–PVA gel. In the 5-FU/Hp@IL-SA–PVA gel, the presence of the C–F stretching peak around 1245 cm^{-1} and the C═O stretching peak near 1706 cm^{-1} in the spectrum strongly supports the successful physical incorporation of 5-FU into the hydrogel matrix.[23] These characteristic peaks, retained from the pure drug spectrum, confirm that 5-FU remains chemically stable within the network and is effectively embedded in the hydrogel structure. Additionally, the broadening or shifting of the N–H and C═O peaks suggests potential hydrogen bonding interactions between the drug and the

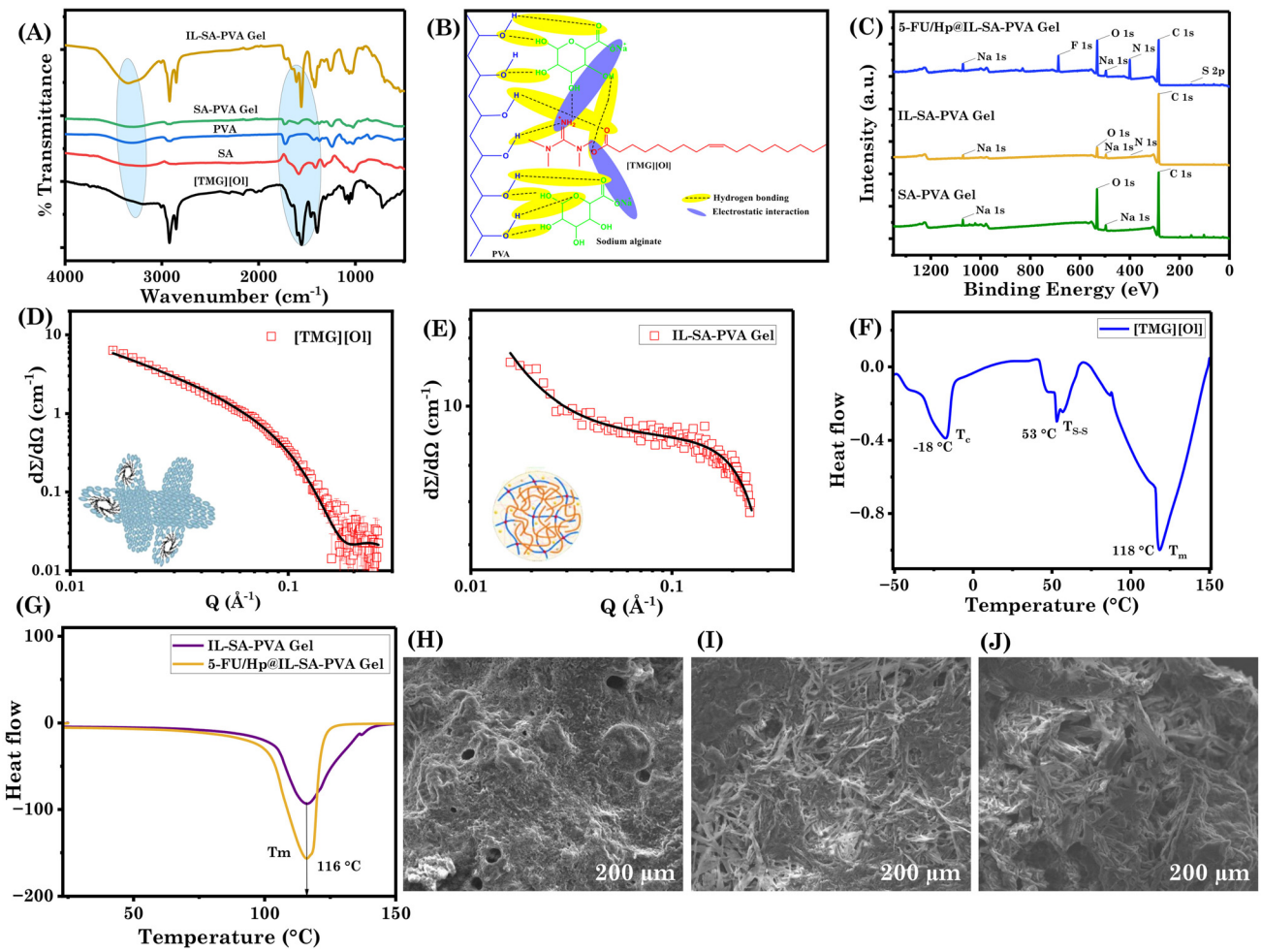

Fig. 1 (A) Comparative FTIR spectra of each component and the prepared hydrogel. (B) Graphical interaction between [TMG][Ol], SA and PVA. (C) Wide scan XPS spectra. SANS graphs of (D) [TMG][Ol] and (E) IL-SA–PVA gel. DSC graphs of the (F) [TMG][Ol], (G) IL-SA–PVA gel and 5-FU/Hp@IL-SA–PVA gel. FE-SEM images of the (H) SA–PVA gel, (I) IL-SA–PVA gel and (J) 5-FU/Hp@IL-SA–PVA gel.

hydrogel network. Hp is likely to interact with the hydrogel, as indicated by the shifts observed in the sulfate (1270 cm^{-1}) and carboxylate (1610 cm^{-1}) stretching vibrations in the 5-FU/Hp@IL-SA–PVA gel, respectively, suggesting the involvement of hydrogen bonding.

The structural modifications and drug loading suggested by the FTIR analysis were further validated through XPS, which provided surface elemental composition and chemical state information of the developed hydrogels, including the SA–PVA gel, IL-SA–PVA gel, and 5-FU/Hp@IL-SA–PVA gel (Fig. 1C). In the SA–PVA gel, the XPS spectrum exhibited peaks corresponding to C 1s, O 1s, and Na 1s, reflecting the presence of the polymeric backbone and sodium ions from sodium alginate. Upon [TMG][Ol] incorporation, the IL-SA–PVA gel displayed an additional N 1s peak along with the existing C 1s, O 1s, and Na 1s peaks. The appearance of N 1s confirms the successful incorporation of the nitrogen-containing IL. The 5-FU/Hp@IL-SA–PVA gel shows new peaks for F 1s and S 2p, in addition to C 1s, O 1s, Na 1s, and N 1s. The presence of F 1s and S 2p peaks confirms the successful loading of 5-FU and Hp into the hydrogel system, corresponding to the fluorine atom and sulfate groups, respectively. Additionally, the XPS atomic content data (Table S2) reveal increased nitrogen and sodium levels in the 5-FU/Hp@IL-SA–PVA gel, further supporting the incorporation of 5-FU and Hp.

In the high-resolution C 1s XPS spectrum (Fig. S5A), three distinct peaks were observed at 288.7 eV (C═O), 286.4 eV (C–O, C–O–C), and 284.5 eV (C–C, C═C, C–H).[15] The O 1s spectrum shows a broad peak at 531.6 eV, corresponding to the oxygen atoms in C═O and C–O (O–C–O and C–OH) groups (Fig. S5B).[16] In the Na 1s spectrum (Fig. S5C), a single peak was observed at 1071 eV. The increased peak intensity in the 5-FU/Hp@IL-SA–PVA gel can be attributed to the presence of sodium ions from Hp, which contribute to the higher sodium content in the hydrogel. A noticeable shift toward lower binding energies across all spectra suggests strong interactions between the incorporated drugs and the hydrogel, potentially involving hydrogen bonding or electrostatic interactions. The F 1s peak at 687.2 eV corresponds to the C–F bond in the 5-FU/Hp@IL-SA–PVA gel (Fig. S5D), confirming the successful incorporation of 5-FU into the hydrogel matrix.[17] In the N 1s spectrum of the IL-SA–PVA gel (Fig. S5E), a characteristic peak is observed around 400.2 eV, which corresponds to the guanidinium group present in [TMG][Ol]. This confirms the successful incorporation of the IL into the hydrogel matrix. Upon loading the drug, the N 1s spectrum shows an increased intensity along with slight shifts and peak broadening, indicating the presence of multiple nitrogen environments. This enhancement arises from the nitrogen atoms in 5-FU and Hp. Additionally, a peak around 405 eV suggests the presence of oxidized nitrogen species.[18] These spectral changes confirm the successful loading of both nitrogen-containing drugs within the IL-functionalized hydrogel. The high-resolution S 2p XPS spectra of the 5-FU/Hp@IL-SA–PVA gel showed three peaks at 172.8 eV (oxidized sulfur), 168.6 eV (sulfonate groups), and 163.2 eV, which may arise from interactions between Hp and the hydrogel matrix, confirming the presence of heparin's characteristic sulfur functionalities (Fig. S5F).[24,25]

By performing SANS measurements (Table 2), we confirmed the hypothesis of a micellar transition driven by synergistic interactions between [TMG][Ol] and the polymeric components. Initially, the [TMG][Ol] solution exhibited rod-like micellar structures with a radius of 22 Å, as evident from the fitting with a micellar model (Fig. 1D). Upon incorporation of SA and PVA, the scattering pattern changed significantly, and the data were better fitted using the correlation length model,[26] suggesting the formation of a hydrogel network (Fig. 1E).

$$I(Q) = \frac{A}{Q_m} + \frac{C}{(1 + Q\xi^m)} + B \quad (3)$$

In eqn (3), the clustering of the gel structure at large length scales is described by the Porod function, which is the first element in this formula. The fractal feature of the hydrogel is described by the Porod exponent m, whereas the incoherent background is B. The Lorentzian function is the second term; specifically, the correlation length of the polymer chains is denoted by ξ, and the Lorentzian exponent is the inverse of the Flory exponent.

The correlation length was found to be approximately 1.36 Å, indicating an increased degree of structural organization and intermolecular interactions. This transition confirms the transformation of [TMG][Ol] micelles into a cross-linked hydrogel matrix *via* cooperative interactions among IL and polymer molecules.

Thermal stability of the hydrogels is a critical parameter in determining their suitability for practical applications, especially in thermally responsive or long-term functional systems. The phase behaviour of pure [TMG][Ol] was investigated using DSC, as shown in Fig. 1F. The thermal transitions, including the crystallization temperature (T_c), solid–solid phase transition temperature (T_{s-s}), and melting point (T_m), were observed at −18 °C, 53 °C, and 118 °C, respectively. The thermal behaviour of the IL-SA–PVA gel and 5-FU/Hp@IL-SA–PVA gel demonstrated a clear thermo-responsive nature, exhibiting a gel-to-sol transition around 116 °C (Fig. 1G). The 5-FU/Hp@IL-SA–PVA gel showed a more pronounced melting transition, indicative of responsive structural rearrangements upon heating. The similarity in transition temperatures for both hydrogels suggests that the incorporation of drugs does not significantly alter the thermo-responsive behaviour of the

Table 2 Fitting parameters of the IL solution and IL-based hydrogel

Sample	Length (Å)	Radius (Å)	Polydispersity	Model
[TMG][Ol]	>500	22.0	0.3	Rod-like micelles
	Correlation length (Å)	**Porod exponent**	**Lorentz exponent**	
IL-SA–PVA gel	1.33	1.73	3.6	Correlation length

hydrogel. This highlights its suitability as a robust and stable platform for drug delivery applications.

The FE-SEM micrographs of the SA–PVA hydrogel exhibited fewer irregularities and a less porous structure (Fig. 1H). The reduced porosity and weaker cross-linking, due to the absence of [TMG][Ol], limit the drug-loading capacity and sustained release potential, highlighting the critical role of the IL in enhancing hydrogel morphology and functionality. An increased crosslinker concentration in SA- and PVA-based systems results in the formation of more porous structures.[27] In the current study, [TMG][Ol] and SA–PVA were physically crosslinked without the use of a crosslinker to create a 3D porous structure. The IL-SA–PVA gel exhibited a rough, uneven surface morphology with noticeable irregularities, as seen in Fig. 1I. Additionally, the image showcased a highly porous architecture characterized by irregularly sized and shaped pores. This porous structure is crucial for improving the drug loading capacity of the hydrogel and ensuring controlled, sustained release, making it highly suitable for drug delivery systems.[28] However, the 5-FU/Hp@IL-SA–PVA gel exhibited enhanced aggregation, likely due to strong intermolecular interactions between the IL-SA–PVA gel and the drugs (5-FU and Hp), which may promote localized network densification upon drug incorporation (Fig. 1J). This indicates that the formation of the drug-loaded hydrogel relies on robust intermolecular interactions, leading to a roughened surface with drug particles integrated into the hydrogel matrix.

3.2. Swelling behaviour of the hydrogel

The IL-SA–PVA hydrogel exhibited pronounced pH-responsive swelling behaviour. Time-resolved swelling studies indicated that the hydrogel swelled more rapidly and to a greater extent at acidic pH (5.2) compared to physiological pH (7.4) (Fig. 2A). The swelling ratio reached approximately 25.7 at pH 5.2 and 14.4 at pH 7.4 after 140 minutes, indicating significant network expansion under acidic conditions. The increased swelling likely facilitated water penetration, resulting in greater network expansion at acidic pH and larger, more open pore structures. These observations indicate that the pore size of the hydrogel is pH-sensitive, increasing under acidic conditions due to enhanced ionization of hydroxyl, amine and carboxyl groups and consequent network expansion.

3.3. Mechanical properties of the hydrogel

A specific level of mechanical strength is necessary for the hydrogel to be suitable for drug delivery applications. We conducted the rheological characterization of the investigated hydrogel in order to assess its mechanical behaviour and performance, especially in the context of biological applications like drug administration and tissue engineering to name a few.[29] To determine the viscoelastic behaviour of hydrogels, a strain sweep test was conducted.[30] The crossover points (γ_c) for SA–PVA and IL-SA–PVA hydrogels were observed at strain values of 2.91% and 6.72%, respectively, as depicted in Fig. 2B. An elastic or linear region is defined as the area below γ_c where G' is greater than G''. The hydrogel acts like a semisolid material in this area. Above γ_c, however, G' is smaller than G'', indicating that the hydrogel was distorted and acts like a viscous solution. Incorporating the IL improves the crossover point of the hydrogel, thereby enhancing its mechanical strength, one of the most important properties if the hydrogel is to be used as a transdermal drug delivery vehicle. Moreover, the mechanical characteristics of hydrogels can be confirmed by the angular frequency sweep test.[30] At a constant strain of 1%, the storage modulus (G') is greater than the loss modulus (G'') in the 0.1 to 100 rad s^{-1} angular frequency range, as shown in Fig. 2C. This result confirmed that the hydrogel is stable or retains its elastic characteristics within this range of angular frequencies.

Furthermore, the viscosity study has been accomplished, exhibiting the flowing nature of hydrogel. The viscosity of the hydrogel reduces as the shear rate rises, suggesting a shear-thinning behaviour (Fig. 2D).[31] At lower shear rates, the hydrogel exhibits high viscosity; as shear rate increases, it displays a flowing characteristic as a result of a decrease in viscosity. These kinds of outcomes support the injectable behaviour of the hydrogel and are considered it for drug delivery.[32] The incorporation of SA into the PVA hydrogel enhanced its rheological properties, showing improved mechanical strength and viscoelastic behaviour compared to the pure PVA hydrogel.[33] Fayyazbakhsh *et al.*[34] developed a hydrogel based on alginate and gelatin and found that adding gelatin improved its shear thinning properties. In the present hydrogel, SA–PVA was used, and the shear-thinning properties were enhanced through the incorporation of [TMG][Ol]. These findings highlight the significant role of the IL in enhancing the structural integrity of the hydrogel and mechanical strength, which is crucial for its performance in drug delivery applications.

It is crucial to research the thixotropic behaviour of the hydrogel in order to employ it as a drug delivery vehicle that can inject the drug through the skin. The thixotropic behaviour of the hydrogel was examined while varying the strain value at a constant frequency (1 rad s^{-1}). As the strain value increased from 0.1% to 25%, the storage modulus decreased from 970 to 310 Pa, indicating that the hydrogel had transformed into a quasi-liquid state. Upon removing the strain, the quasi-liquid state transformed into the quasi-solid state and the storage modulus returned to its initial value for up to 6 cycles (Fig. 2E). This investigation validates the injectable and self-healing properties of the hydrogel.[35] The gel must regain its dynamic moduli once strain is released and flow as a liquid when pressure is applied in order to become injectable. The above-described thixotropic behaviour results validate the injectability of the hydrogels being studied.[36]

Furthermore, injecting the hydrogel at a specific target spot is required for targeted drug delivery. The hydrogel under investigation transforms into a sol state under considerable shear strain, according to the rheological parameters. Through the incorporation of drug molecules into the gel matrix, we hope to investigate the possibility of using the hydrogel as an injectable gel for localized treatment. This requires that the applied shear strain fall within the syringe's compressed plunger range in order to ensure proper flow and recovery. As a

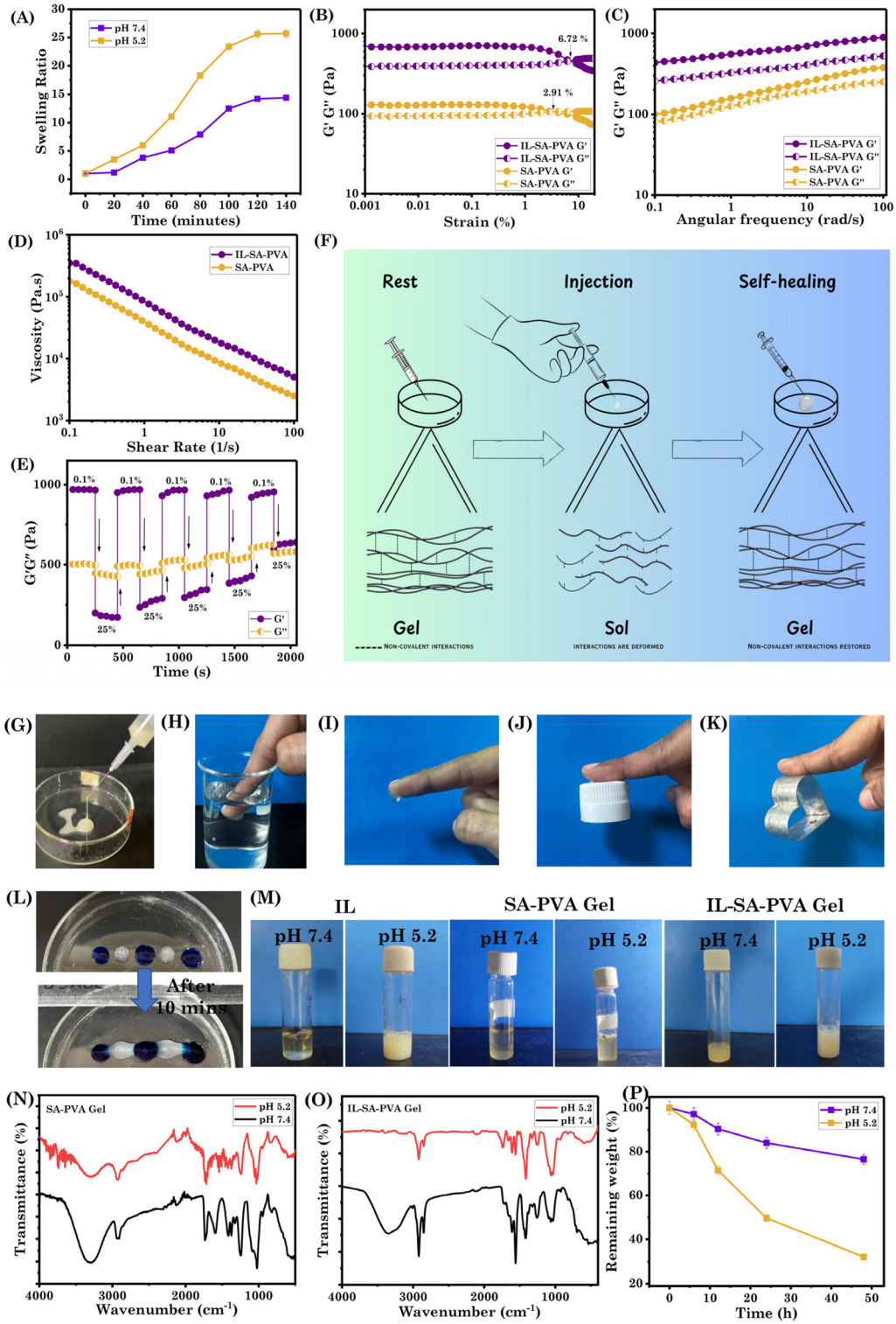

Fig. 2 (A) Swelling kinetics of the IL-SA–PVA gel. (B) Strain sweep with a constant frequency of 1 rad s^{-1}. (C) Frequency sweep data of hydrogels at a constant strain of 0.1%. (D) Viscosity measurement. (E) Thixotropic data. (F) Schematic illustration of the mechanism of action of the injectable hydrogel. (G) Visual image of the injectable hydrogel; adhesive characteristics with (H) skin in water, (I) skin, (J) plastic and (K) metal in air. (L) Visual images of the self-healing properties of the hydrogel. (M) Visual observation of the IL, SA–PVA gel and IL-SA–PVA gel at neutral to acidic pH. FTIR spectra of the (N) SA–PVA gel, (O) IL-SA–PVA gel and (P) *in vitro* degradation with pH.

result, the gel acts like a liquid, passing through the needle and returning to its original form when the strain is released. When a 27-gauge needle was used to release the plunger after adding hydrogel to the 10 mL syringe, 53 psi of pressure was produced.[37] We found that the hydrogel flows like a liquid when pressure is applied through the syringe plunger, disrupting the hydrogen bonding network, and that it returns to its initial shape when the pressure is released (Fig. 2G). A schematic representation of the mechanism of the injectable hydrogel is illustrated in Fig. 2F.

In biological applications including wound healing, drug delivery, and tissue engineering, the adhesive ability of the hydrogel is essential. The IL-SA–PVA gel exhibits outstanding adhesiveness to a variety of surfaces, including skin, plastic, metal and underwater with skin, as shown in Fig. 2H–K. The adhesive nature of the hydrogel arises from functional groups like –OH, –NH and $–COO^-$, which enable noncovalent interactions with the functional groups on the surfaces of various materials.[38]

3.4. Self-healing properties of the hydrogel

At various phases, self-healing relies significantly on chemical and physical bonds. If a hydrogel is going to be employed for drug delivery, it must be able to repair itself. Reversible chemistry is important for the hydrogel-based systems because it enables the broken gel network to be collectively repaired, completing the self-healing process. One of the characteristics of the hydrogen bond is that it reforms quickly after breaking, which gives self-healing its early traction. Since ILs facilitate electrostatic interactions within the hydrogel matrix, the IL-based hydrogel exhibits an enhanced self-healing capability.[39] To further investigate the self-healing properties, the hydrogel was sliced into separate pieces, and opposing sections were rejoined to observe whether they could seamlessly self-heal. After 10 minutes, the IL-SA–PVA hydrogel was seen to self-heal without any external assistance, highlighting the crucial role of [TMG][Ol] (Fig. 2L).

3.5. *In vitro* degradation with pH

If a hydrogel is utilized as an implant or injection, it must be removed from the body after drug delivery or degrade into biocompatible and non-toxic components under physiological conditions. As shown in Fig. 2M, the study examined the degradation of the hydrogel under normal (pH 7.4) and tumor cell conditions (pH 5.2). After immersion in PBS buffer at pH 7.4, the physical appearance of the hydrogel remained unchanged until day 7. However, when the IL-SA–PVA gel was incubated in PBS buffer at pH 5.2, turbidity in the solution was observed after 1 day, possibly indicating the disruption of the 3D network of the hydrogel due to the conversion of oleate ions into oleic acid. To further support this, parallel experiments were conducted using [TMG][Ol] and the SA–PVA gel. It was observed [TMG][Ol] began to precipitate at pH 5.2, likely due to the protonation of oleate ions into oleic acid. In contrast, the SA–PVA gel remained stable under the same acidic conditions, showing no notable changes in appearance.

Furthermore, FTIR spectroscopy was employed to investigate the structural stability of SA–PVA and IL-SA–PVA hydrogels at neutral and acidic pH (Fig. 2N and O). The SA–PVA gel displayed minimal spectral changes, indicating good chemical stability. Minor shifts were observed in the asymmetric and symmetric stretching vibrations of the carboxylate groups at 1602 and 1410 cm^{-1}, likely due to partial protonation. The broad O–H stretching band (3290 cm^{-1}) showed negligible variation, suggesting that the hydrogen-bonded network remained largely intact. While the IL-SA–PVA gel exhibited significant spectral changes upon acidic treatment. A distinct new peak appeared around 1733 cm^{-1}, corresponding to the C=O stretching of carboxylic acid, confirming the conversion of oleate ions to oleic acid. Additionally, the reduction in the intensity of the carboxylate peaks and changes in the alkyl chain stretching region (2848–2923 cm^{-1}) indicated the degradation and partial precipitation of [TMG][Ol]. These findings support the pH-responsive behaviour of the IL-SA–PVA gel and its tendency toward network disruption under acidic conditions.

As shown in Fig. 2P, the IL-SA–PVA gel demonstrated a markedly faster degradation rate under acidic conditions (pH 5.2) compared to physiological pH (7.4). After 48 hours, the remaining weight of the hydrogel was approximately 32.1% at pH 5.2 and 76.5% at pH 7.4, indicating its pH-responsive degradability and potential suitability for controlled drug release in acidic microenvironments such as tumor tissues.

3.6. *In vitro* biocompatibility assay using HaCaT cells

Biocompatibility is an important element in drug delivery systems; a system with low biocompatibility might negatively impact healthy cells or tissues. We verified this remark by conducting an *in vitro* biocompatibility test of the hydrogel with normal cell lines (HaCaT cells). Fig. 3A shows that HaCaT cell viability remained above 95% for 48 hours at varying hydrogel doses. This is because the hydrogel was prepared from biocompatible substances like [TMG][Ol], SA and PVA.[2,19,40] Fig. 3D shows the control image for HaCaT cells, and Fig. 3E and F depict the cell viability following a 48-hour treatment with the hydrogel at 1000 μg ml^{-1}.

3.7. Application of the hydrogel

3.7.1. Loading and sustained release of 5-FU and Hp. The injectable properties of the hydrogel lead us to investigate its potential for medicinal applications by adding drugs into its matrix. The developed IL-SA–PVA hydrogel was evaluated for its potential as a dual drug delivery platform for the loading and sustained release of 5-FU, a widely used chemotherapeutic agent, and Hp, an anticoagulant known for its anti-metastatic properties. The rational design of this hydrogel matrix enables the co-loading of both drugs, resulting in a synergistic therapeutic approach for cancer treatment and metastasis inhibition. The loading efficiency of the IL-SA–PVA gel was evaluated, revealing that it successfully loaded 33.4 mg of 5-FU and 22.6 mg of Hp, corresponding to approximately a 2.5-fold increase compared to the SA–PVA hydrogel. The ionic nature of

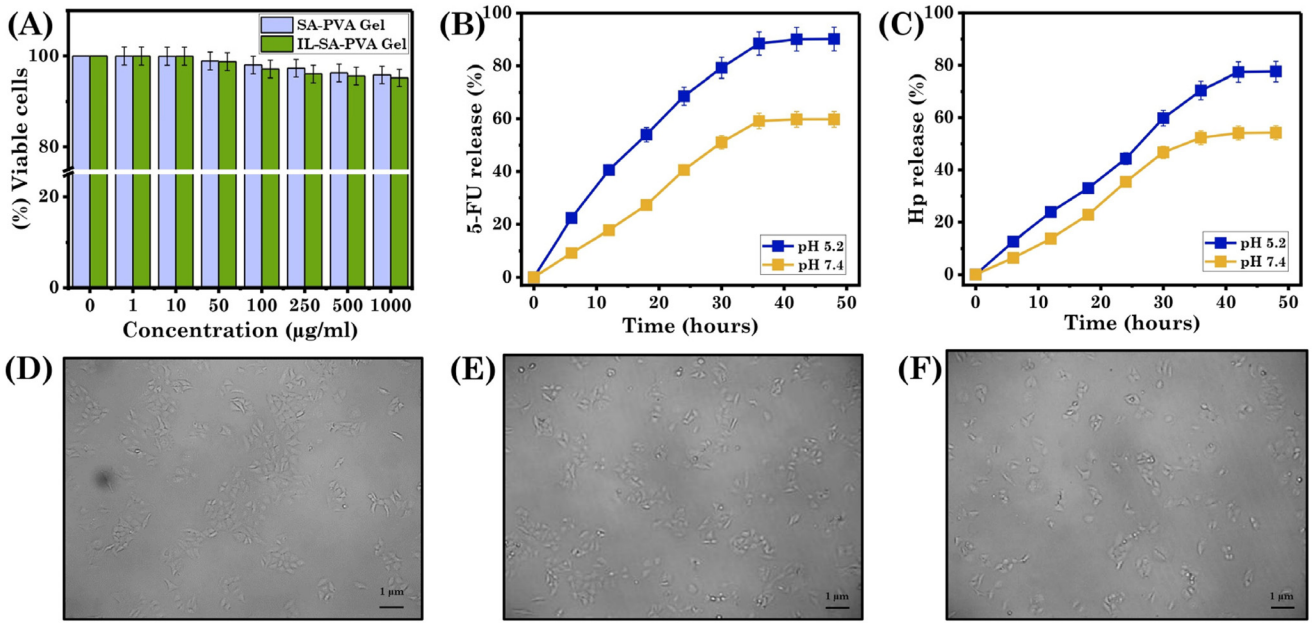

Fig. 3 (A) The cell viability of HaCaT cells by MTT assays after 48 h upon treatment with hydrogels. Drug release (%) of (B) 5-FU and (C) Hp. HaCaT cells (D), control (E), SA–PVA gel and (F) IL-SA–PVA gel (scale: 1 μm).

[TMG][Ol] enhances the hydrophilicity of the hydrogel, leading to improved loading effectiveness of the hydrogel.

The *in vitro* release profile of the drugs that were loaded in the hydrogel matrix was further assessed. The *in vitro* release profile of 5-FU and Hp from the hydrogel was evaluated at 37 °C under two different pH conditions: 5.2 and 7.4 (Fig. 3B and C). For 5-FU, the hydrogel exhibited a release of 90.2% at pH 5.2 and 59.8% at pH 7.4, whereas Hp showed a release of 77.6% and 54.2% under the same respective pH conditions. The enhanced drug release at pH 5.2 compared to pH 7.4 can be attributed to the pH-responsive nature of [TMG][Ol] incorporated into the hydrogel matrix. Under acidic conditions, the protonation of functional groups within the IL network may lead to increased swelling or disruption of the hydrogel structure, thereby facilitating faster drug diffusion. Moreover, 5-FU exhibited a higher release than Hp, attributed to its significantly smaller molecular size and higher diffusivity compared to the large, highly charged Hp molecules. Initially, a burst release of 5-FU was observed, followed by a sustained release pattern of Hp. The sustained release profile of the hydrogel is expected to maintain a high local concentration of drugs in the surrounding tissues over an extended treatment period.

Understanding the mechanism of mass transport during drug release is critical for determining how therapeutic agents are delivered into the body to facilitate effective therapy. To successfully optimize the performance of the delivery vehicle, it is necessary to study the drug release pattern and statistically anticipate the release kinetics. Recently, mathematical models have been applied to evaluate the significant physical parameters by model fitting using practical release. To better understand 5-FU and Hp release, we analysed the data using multiple kinetic models (Table S3). Korsmeyer–Peppas provided the best fit for 5-FU at pH 7.4 and for Hp at both pH values (pH 5.2 and 7.4), whereas the release of 5-FU at pH 5.2 followed the Higuchi model more closely (Fig. S6). For the Korsmeyer–Peppas fits, the exponent n was used to infer the release mechanism for our slab geometry: $n \leq 0.5$ indicates Fickian diffusion, $0.5 < n < 1$ denotes anomalous (diffusion + polymer relaxation) transport, and $n \approx 1$ corresponds to Case-II (relaxation/erosion)-controlled release.[41] We observed that the 5-FU/Hp@IL-SA–PVA gel exhibited n values between 0.5 and 1, indicating a non-Fickian or anomalous transport mechanism. The Higuchi fit for 5-FU at pH 5.2 indicates diffusion-controlled release with square-root-of-time dependence.[42] The differences imply that acidic conditions have affected drug-matrix or swelling behaviour, with simple diffusion dominating for 5-FU at pH 5.2 and mixed mechanisms governing release in the other instances. This ensures that the drugs are released gradually in a sustained manner over an extended period, rather than being released rapidly at once.

3.7.2. *In vitro* cytotoxicity of the hydrogel. The IL-SA–PVA hydrogel exhibited excellent biocompatibility, with minimal cytotoxic effects on normal cells, as indicated by the preceding data. The cytotoxicity of the 5-FU/Hp@IL-SA–PVA gel was evaluated on HaCaT cells to assess its cytocompatibility. The hydrogel showed approximately 53.5% cell viability at the highest tested concentration (25 μg mL^{-1}), indicating moderate cytotoxicity (Fig. 4A). Although the encapsulated drug (5-FU) is intrinsically cytotoxic, its controlled and limited release at physiological pH (7.4) substantially minimized its cytotoxicity to normal cells. This indicates that the hydrogel matrix acts as

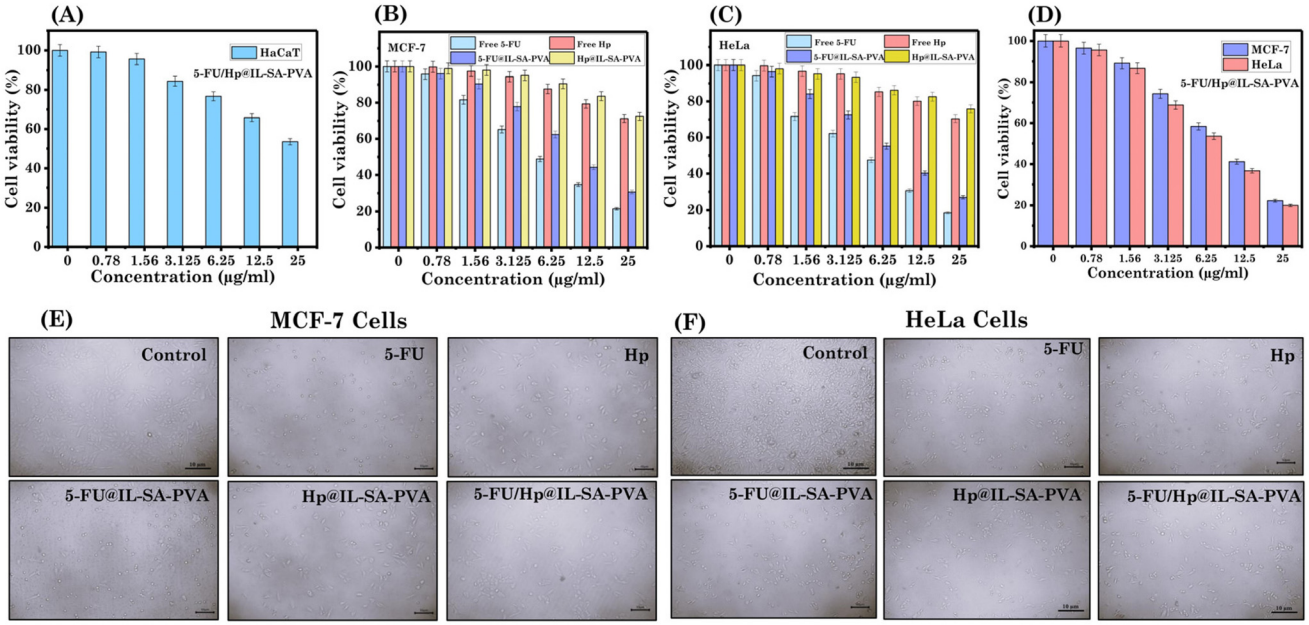

Fig. 4 *In vitro* cytotoxicity of the hydrogel on the (A) HaCaT, (B) MCF-7 and (C) HeLa cells. (D) *In vitro* cytotoxicity of the 5-FU/Hp@IL-SA–PVA gel on the MCF-7 and HeLa cells. Images of (E) MCF-7 cells and (F) HeLa cells after treatment (scale: 10 μm).

a protective barrier, allowing for prolonged and localized drug release, particularly at the diseased location, while retaining adequate cytocompatibility under physiological conditions. A microscopic image of HaCaT cells after treatment with the 5-FU/Hp@IL-SA–PVA gel is shown in Fig. S7.

An *in vitro* cytotoxicity study was utilized to determine the effectiveness and required dose of 5-FU/Hp-loaded hydrogels for tumor cell suppression.[43] For this objective, we utilized MCF-7 (breast carcinoma) and HeLa (cervical cancer) cell lines for our experiments. To evaluate the cytotoxicity and potential synergistic effects of the 5-FU/Hp@IL-SA–PVA hydrogel, MCF-7 and HeLa cells were treated with free 5-FU, free Hp, 5-FU@IL-SA–PVA hydrogel, Hp@IL-SA–PVA hydrogel, and the combined 5-FU/Hp@IL-SA–PVA hydrogel. As expected, free 5-FU exhibited high cytotoxicity toward both cancer cell lines, resulting in low IC_{50} values (MCF-7: 6.11 μg mL^{-1}; HeLa: 5.94 μg mL^{-1}), whereas free heparin showed negligible cytotoxicity, confirming its biocompatibility (Fig. 4B and C).

The 5-FU@IL-SA–PVA hydrogel showed moderate cytotoxicity, with higher IC_{50} values (MCF-7: 7.49 μg mL^{-1}; HeLa: 6.84 μg mL^{-1}) than free 5-FU, consistent with the sustained and controlled drug release from the hydrogel matrix. The Hp@IL-SA–PVA hydrogel did not significantly affect cell viability (Fig. 4B and C). Importantly, the 5-FU/Hp@IL-SA–PVA hydrogel exhibited enhanced cytotoxicity compared to the single-drug hydrogels at equivalent concentrations, confirming the synergistic effect of the dual-drug formulation. After 48 hours of treatment with the 5-FU/Hp@IL-SA–PVA hydrogel, the IC_{50} values were determined to be 7.15 μg mL^{-1} for the MCF-7 cell line and 6.67 μg mL^{-1} for the HeLa cell line, as shown in Fig. 4D. These findings suggest that the system exhibits substantial cytotoxicity against cancer cell lines at low doses (Fig. 4E and F).

3.7.3. *In vitro* cell migration assay. Cell migration is a fundamental process involved in various physiological and pathological events such as cancer progression, tissue growth, wound repair, inflammatory responses, and cellular differentiation. The cell culture wound closure experiment was used to evaluate *in vitro* cell motility and migratory capabilities.[44] To assess the *in vitro* inhibitory potential of the 5-FU/Hp@IL-SA–PVA gel, a scratch assay was conducted on HeLa cells. The extent of wound closure was monitored at regular intervals for up to 48 hours following treatment with a 2 μg mL^{-1} concentration of the 5-FU/Hp@IL-SA–PVA gel, allowing the evaluation of its inhibitory effects on cell migration. As illustrated in Fig. 5B, treatment with the 5-FU/Hp@IL-SA–PVA gel resulted in a notable reduction in cell migration into the scratched area. A considerable number of cells were observed within the wound region in both the control and IL-SA–PVA gel, in which the number of cells crossing into the scratched zone was relatively higher than that in the 5-FU/Hp@IL-SA–PVA gel. At 48 hours post-scratching, cells treated with 5-FU/Hp@IL-SA–PVA left around 57.8% of the wound area unclosed, indicating reduced migratory activity. In contrast, only about 29.5% and 34.8% of the scratched area remained uncovered in the control and IL-SA–PVA gel, respectively (Fig. 5A). This means the wound area closure was approximately 1.96 times higher in the control and 1.66 times higher in the IL-SA–PVA gel compared to the 5-FU/Hp@IL-SA–PVA gel, highlighting its strong anti-migratory effect. Overall, the findings demonstrate that the 5-FU/Hp@IL-SA–PVA gel, by combining the migratory inhibitory effects of Hp and the anticancer activity of 5-FU,[45,46] effec-

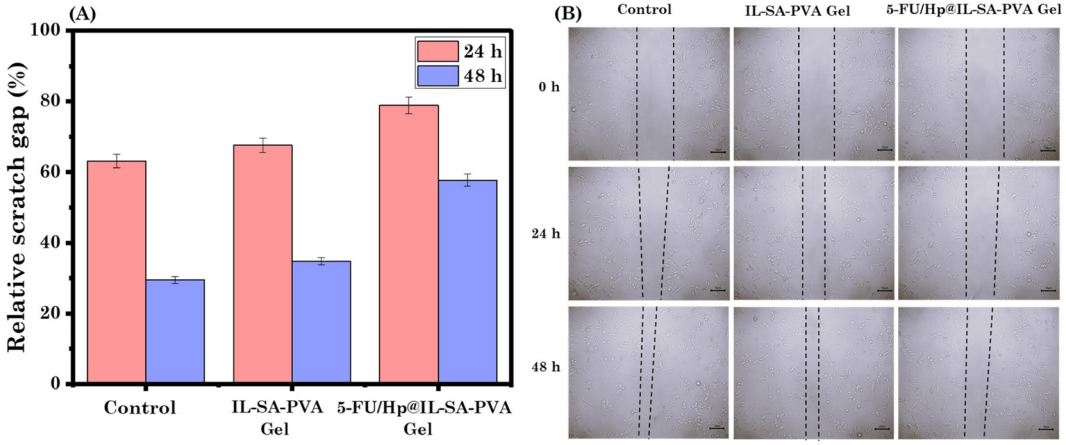

Fig. 5 (A) Based on the initial wound area at 0 hours, the relative migrating cell area was determined using image analysis software. (B) Microscopic images from an *in vitro* scratch assay on HeLa cell cultures (scale: 10 μm).

tively reduces HeLa cell migration, suggesting its potential as a promising candidate for anti-metastatic therapy.

4. Conclusions

In summary, a multifunctional hydrogel was successfully developed by the synergistic interaction between [TMG][Ol], PVA and SA (a biopolymer) for the co-delivery of two therapeutic agents: 5-FU, an anticancer drug, and Hp, known for its anti-metastatic properties. Comprehensive characterization using FTIR, XPS, SANS, FE-SEM and DSC confirmed the successful incorporation of [TMG][Ol] and the drugs (5-FU and Hp) within the hydrogel network. Rheological analysis demonstrated excellent mechanical strength, while thixotropic studies confirmed the injectability of the 5-FU/Hp@IL-SA–PVA gel, making it suitable for minimally invasive administration. Moreover, the hydrogel exhibited desirable self-healing and adhesive properties, essential for biomedical applications. Notably, the presence of [TMG][Ol] significantly enhanced the drug loading capacity of the hydrogel, showing approximately a 2.5-fold increase compared to hydrogels without [TMG][Ol]. The pH-responsive behaviour imparted by [TMG][Ol] facilitated a controlled and sustained release of both drugs specifically at acidic pH (5.2), mimicking the tumor microenvironment, with over 90.2% of 5-FU and 77.6% of Hp released within 48 hours. Biocompatibility assessment using HaCaT cells revealed the non-toxic nature of the hydrogel carrier. Importantly, *in vitro* cytotoxicity studies against MCF-7 and HeLa cancer cell lines confirmed significant anticancer efficacy, and *in vitro* anti-metastatic activity evaluated using HeLa cells demonstrated promising therapeutic potential. Overall, the developed IL-SA–PVA hydrogel presents a promising platform for targeted, pH-responsive, and dual-drug delivery with potential applications in cancer therapy and metastasis inhibition.

Author contributions

Ishani Pandya: conceptualization, methodology, writing – original draft and visualization. Vidhi Joshi: methodology and writing – original draft. Sugam Kumar: methodology and writing – original draft. Vinod K. Aswal: methodology and writing – original draft. Naina Raje: methodology and writing – original draft. Muzammil Kuddushi: methodology and writing – original draft. Xuehua Zhang: revising the draft. Naved Malek: conceptualization, supervision, writing – review and editing, and funding acquisition. All authors have given approval to the final version of the manuscript.

Conflicts of interest

There are no conflicts to declare.

Data availability

Data will be made available upon request. Supplementary information (SI) is available. See DOI: https://doi.org/10.1039/d5nr03333k.

Acknowledgements

N. M. acknowledges the financial assistance received from UGC-DAE-CSR under the Collaborative Research Scheme (UDCSR/MUM/AO/CRS-M-997/2023).

References

1 X. Jiang, N. Xiang, H. Zhang, Y. Sun, Z. Lin and L. Hou, *Carbohydr. Polym.*, 2018, **186**, 377–383.

2 I. Pandya, H. Ukani, V. Joshi, M. Kuddushi, X. Zhang, N. Raje and N. Malek, *Mater. Today Chem.*, 2025, **45**, 102674.
3 I. Pandya, V. Joshi, M. Kuddushi, X. Zhang, S. Kumar, V. K. Aswal, N. H. Raje and N. Malek, *ACS Appl. Eng. Mater.*, 2025, **3**, 1819–1833.
4 R. Pansuriya, T. Patel, K. Singh, A. Al Ghamdi, N. Kasoju, A. Kumar, S. K. Kailasa and N. I. Malek, *Int. J. Biol. Macromol.*, 2024, **277**, 134112.
5 F. Martínez-Gómez, J. Guerrero, B. Matsuhiro and J. Pavez, *Carbohydr. Polym.*, 2017, **155**, 182–191.
6 H. Anwar, M. Ahmad, M. U. Minhas and S. Rehmani, *Carbohydr. Polym.*, 2017, **166**, 183–194.
7 R. Pansuriya, T. Patel, S. Mehra, A. Kumar, O. A. El Seoud, S. Kumar, V. K. Aswal, S. K. Kailasa and N. I. Malek, *New J. Chem.*, 2023, **47**, 14261–14272.
8 A. Sheikhi, S. Afewerki, R. Oklu, A. K. Gaharwar and A. Khademhosseini, *Biomater. Sci.*, 2018, **6**, 2073–2083.
9 H.-L. Tan, S.-Y. Teow and J. Pushpamalar, *Bioengineering*, 2019, **6**, 17.
10 R. Pansuriya, J. Doutch, B. Parmar, S. K. Kailasa, N. Mahmoudi, C. Hoskins and N. I. Malek, *J. Mater. Chem. B*, 2024, **12**, 5479–5495.
11 H. Rashidzadeh, S. J. Tabatabaei Rezaei, H. Danafar and A. Ramazani, *J. Drug Delivery Sci. Technol.*, 2022, **76**, 103740.
12 H. Rashidzadeh, A. Ramazani, S. J. T. Rezaei, H. Danafar, S. Rahmani, H. Veisi, M. Rajaeinejad, Z. Jamalpoor and Z. Hami, *J. Biomater. Sci., Polym. Ed.*, 2023, **34**, 1824–1842.
13 Y.-Y. Chen, H.-C. Wu, J.-S. Sun, G.-C. Dong and T.-W. Wang, *Langmuir*, 2013, **29**, 3721–3729.
14 C. N. Zhu, S. Y. Zheng, H. N. Qiu, C. Du, M. Du, Z. L. Wu and Q. Zheng, *Macromolecules*, 2021, **54**, 8052–8066.
15 X. Chen, X. Wang and D. Fang, *Fullerenes, Nanotubes and Carbon Nanostruct.*, 2020, **28**, 1048–1058.
16 Y. Peng, Z. Chen, R. Zhang, W. Zhou, P. Gao, J. Wu, H. Liu, J. Liu, A. Hu and X. Chen, *Nano-Micro Lett.*, 2021, **13**, 192.
17 X. L. Zhu, S. B. Liu, B. Y. Man, C. Q. Xie, D. P. Chen, D. Q. Wang, T. C. Ye and M. Liu, *Appl. Surf. Sci.*, 2007, **253**, 3122–3126.
18 I. Matanovic, K. Artyushkova, M. B. Strand, M. J. Dzara, S. Pylypenko and P. Atanassov, *J. Phys. Chem. C*, 2016, **120**, 29225–29232.
19 I. Pandya, S. Mishra, T. Patel, N. Keppeler, S. Kumar, V. K. Aswal, S. Kumar Kailasa, O. El Seoud and N. I. Malek, *J. Mol. Liq.*, 2024, **409**, 125443.
20 National Center for Biotechnology Information, PubChem Compound Summary for CID 66460, 1,1,3,3-Tetramethylguanidine, accessed 13th October, 2025.
21 ChemicalBook, Oleic acid (CAS 112-80-1) ^{1}H NMR spectrum, accessed 13 October, 2025.
22 P. K. Khatri, M. S. Athira, G. D. Thakre and S. L. Jain, *Mater. Sci. Eng., C*, 2018, **91**, 208–217.
23 D. L. Melnikova, Z. F. Badrieva, M. A. Kostin, C. Maller, M. Stas, A. Buczek, M. A. Broda, T. Kupka, A.-M. Kelterer, P. M. Tolstoy and V. D. Skirda, *Molecules*, 2020, **25**, 5706.
24 M. Goh, K. Min, Y. H. Kim and G. Tae, *RSC Adv.*, 2024, **14**, 1866–1874.
25 L. Qie, W. Chen, X. Xiong, C. Hu, F. Zou, P. Hu and Y. Huang, *Adv. Sci.*, 2015, **25**, 1500195.
26 B. Hammouda, D. L. Ho and S. Kline, *Macromolecules*, 2004, **37**, 6932–6937.
27 L. R. Shivakumara and T. Demappa, *Turk. J. Pharm. Sci.*, 2019, **16**, 252–260.
28 S. A. P. Siboro, D. S. B. Anugrah, K. Ramesh, S.-H. Park, H.-R. Kim and K. T. Lim, *Carbohydr. Polym.*, 2021, **260**, 117779.
29 I. Pandya, S. Kumar, V. K. Aswal, O. El Seoud, M. A. Assiri and N. Malek, *Int. J. Pharm.*, 2024, **658**, 124206.
30 G. Stojkov, Z. Niyazov, F. Picchioni and R. K. Bose, *gels*, 2021, **7**, 255.
31 M. Guvendiren, H. D. Lu and J. A. Burdick, *Soft Matter*, 2012, **8**, 260–272.
32 M. H. Chen, L. L. Wang, J. J. Chung, Y.-H. Kim, P. Atluri and J. A. Burdick, *ACS Biomater. Sci. Eng.*, 2017, **3**, 3146–3160.
33 R. Pansuriya, S. Mehra, A. Kumar, O. El Seoud, S. K. Kailasa and N. Malek, *J. Mol. Liq.*, 2023, **382**, 121857.
34 F. Fayyazbakhsh, M. J. Khayat and M. C. Leu, *Int. J. Bioprint.*, 2022, **8**, 618.
35 Z. Li, Y.-M. Zhang, H.-Y. Wang, H. Li and Y. Liu, *Macromolecules*, 2017, **50**, 1141–1146.
36 M. Kuddushi, D. Ray, V. Aswal, C. Hoskins and N. Malek, *ACS Appl. Bio Mater.*, 2020, **3**, 4883–4894.
37 W. Hayward, L. Haseler, L. Kettwich, A. Michael, W. Sibbitt and A. Bankhurst, *Scand. J. Rheumatol.*, 2011, **40**, 379–382.
38 H. Jung, M. K. Kim, J. Y. Lee, S. W. Choi and J. Kim, *Adv. Funct. Mater.*, 2020, **30**, 2004407.
39 Y. Wang, Y. Jia, H. Ren, C. Lao, W. Peng, B. Feng and J. Wang, *Mater. Today Bio*, 2021, **12**, 100138.
40 K. Y. Lee and D. J. Mooney, *Prog. Polym. Sci.*, 2012, **37**, 106–126.
41 R. W. Korsmeyer, R. Gurny, E. Doelker, P. Buri and N. A. Peppas, *Int. J. Pharm.*, 1983, **15**, 25–35.
42 T. Higuchi, *J. Pharm. Sci.*, 1963, **52**, 1145–1149.
43 M. A. Safwat, G. M. Soliman, D. Sayed and M. A. Attia, *Mol. Pharm.*, 2018, **15**, 2194–2205.
44 Z. Chen, T. He, K. Zhao and C. Xing, *Oncol. Lett.*, 2017, **13**, 655–660.
45 A. T. Andrgie, S. L. Mekuria, K. D. Addisu, B. Z. Hailemeskel, W. Hsu, H. Tsai and J. Lai, *Macromol. Biosci.*, 2019, **19**, 1800409.
46 J. Sang, R. Tang, M. Yang and Q. Sun, *BioMed. Res. Int.*, 2020, 1–9.